ACI STRUCTURAL JOURNAL TECHNICAL PAPER

Title No. 115-S138

Punching Tests of Double-Hooked-End Fiber-Reinforced Concrete Slabs

by K. Chanthabouala, S. Teng, J. Chandra, K.-H. Tan, and C. P. Ostertag

Ten high-strength concrete slabs reinforced with a new type of steel fiber, double-hooked-end steel fibers, were tested under punching shear loads. The strength of the concrete f_c' *varied from 80 to 100 MPa (11,600 to 14,500 psi). The fiber content* V_f *varied from 0 to 1.2%. Two different values of flexural reinforcement ratios* ρ *(=* A_s/bd*) of 0.9% and 1.4% were chosen for this test program. The experimental results showed that the use of double-hooked-end steel fibers in concrete enhances slab performance significantly in many ways. As the fiber volume or fiber content* V_f *increased, the flexural stiffness of the slab throughout loading history also increased, while both the deflections and crack widths decreased considerably. At the ultimate load stage, the punching shear strength increased by up to 156% compared to non-fibrous concrete slabs. The increase in punching shear strength is significantly higher than the increase introduced by conventional single hooked-end steel fibers. The ductility of the slabs was also significantly improved.*

Comparisons between design methods with experimental results show that the design method from The Concrete Society's TR-34 performs very well. Another method that was based on the yield line theory overestimates the strengths of the slabs. Model Code 2010 method also overestimates the punching shear strengths. Finally, some relevant design recommendations are given.

Keywords: building codes; double-hooked-end fibers; fiber contents; fiber-reinforced concrete; flexural strength; high-strength concrete; punching shear strength; slabs; steel fiber-reinforced concrete.

INTRODUCTION

The use of steel fiber-reinforced concrete (SFRC) can effectively solve some critical design issues concerning ultimate performance (that is, punching shear strength) and serviceability (that is, deflections and cracks). Some of the advantages of SFRC slabs over conventional reinforced concrete (RC) slabs are[1-8]: 1) faster construction times and lower labor costs due to time saved from detailing works of reinforcement (in actual projects, steel fibers have already been used to partially or entirely replace conventional steel bars for both flexural and shear reinforcements); 2) lower risk of durability problems because steel fibers can prevent and control cracks; and 3) better strength and ductility due to superior post-crack behavior of SFRC compared to non-fibrous concrete.

Although SFRC has been widely used in practice in the past decades, the development of standard design procedures is still insufficient. Major building codes such as ACI 318-14[9] and Eurocode 2[10] have yet to implement any design provisions for SFRC structures. Nevertheless, there are available code-like design guidelines and recommendations for design and analysis of SFRC slabs, such as ACI 544.6R by ACI Committee 544,[1] Technical Report 34 (TR-34) by UK's Concrete Society,[4] and Model Code 2010.[11]

The main functions of fibers are to bridge and resist crack openings through pullout resistance mechanism.[12,13] This post-cracking characteristic of SFRC allows the presence of concrete tensile stresses and tensile strains across crack openings, which are omitted in the analysis of conventional, non-fibrous, RC elements. Therefore, theoretically, the post-cracking tensile strength of SFRC enhances the ultimate strength of a concrete section, be it shear strength or flexural strength. Observations from past experiments[14-23] show that the addition of single-hooked-end steel fibers can increase the punching shear strengths of slabs by 40 to 65% compared to those of non-fibrous slabs, depending on the types and volume fractions of the fibers. Analytically, it has been known that increases in shear and flexural strengths due to the inclusion of steel fibers are dependent upon the residual tensile strengths of the SFRC.[4,24] The residual tensile strengths can be obtained from the flexural tests done, for example, according to EN 14651.[25] Both the ultimate punching shear strengths and flexural strengths can be reasonably correlated with several parameters such as fiber volume fractions, fiber shapes, and fiber aspect ratios (ratio of fiber length to diameter). Therefore, these parameters—such as fiber volume fraction V_f and fiber aspect ratio (L_f/D_f)—have become basic variables in most of existing design methods for SFRC structural elements. Several researchers[26,27] also attempted to develop analytical models for predicting the punching shear strength of SFRC slabs based on experimental observations. Therefore, to ensure reliable and safe design procedures, a broader range of SFRC slab data is still needed for verifying existing design methods, as well as for supporting ongoing development of new design approaches.

This paper presents the punching shear tests of 10 steel fiber-reinforced, high-strength concrete slabs. The slab specimens have two different flexural reinforcement ratios ρ (= A_s/bd) of 0.9% and 1.4% and varying steel fiber volume fractions V_f of up to 1.2%. A new type of steel fiber (the double-hooked-end steel fibers[28] shown in Fig. 1(a)) was investigated. The concrete used in the test program had compressive strengths f_c' between 80 and 100 MPa (11,600 and 14,500 psi). The experimental results were then used to verify the applicability of the yield line theory,[29] Model Code 2010 method,[11] and TR-34 method.[4] Some design recommendations derived from this experiment will also be given.

ACI Structural Journal, V. 115, No. 6, November 2018.

MS No. S-2017-425.R1, doi: 10.14359/51706891, was received November 14, 2017, and reviewed under Institute publication policies.

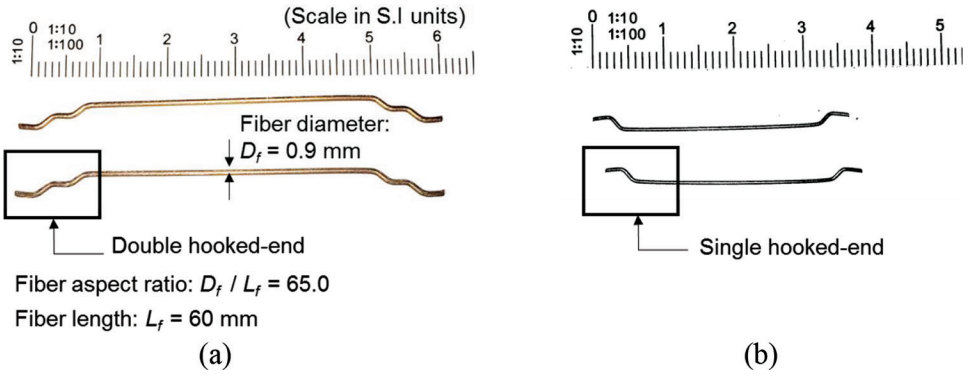

Fig. 1—(a) Double hooked-end steel fiber and its geometric properties; and (b) single (normal) hooked-end steel fiber. (Note: Dimensions in mm; 1 mm = 0.0394 in.)

RESEARCH SIGNIFICANCE

Experimental data of new SFRC slabs are presented. A new type of high-performance steel fibers, the double-hooked-end steel fibers, was used and its influence on punching shear strength was evaluated. The results were discussed in this paper and used to verify the applicability of the yield line theory-based method, Model Code 2010[11] method, and Concrete Society TR-34[4] method. It is expected that this study can provide a useful set of data and new discussions on the development of SFRC slab design method.

EXPERIMENTAL PROGRAM

The dimensions of the specimens represent a typical model taken out of flat-plate slabs supported on square columns, having a column-to-column span of approximately 5.0 to 6.0 m (16.5 to 20 ft). Two main parameters were investigated:

1. Fiber-volume fraction (V_f) or fiber content. Fiber contents of 0%, 0.3%, 0.6%, 0.9%, and 1.2% were used in these slabs to investigate their effectiveness. The equivalent fiber dosages are 0, 23.4, 46.8, 70.2, and 93.6 kg/m^3 (0, 1.46, 2.92, 4.38, and 5.84 lb/ft^3), respectively.

2. Flexural reinforcement ratio ρ (= A_s/bd). Two reinforcement ratios, 0.9% and 1.40%, were considered. The two values of reinforcement ratios were selected to ensure brittle punching shear failure for similar slab specimens but without steel fiber.

Table 1 summarizes the properties of the 10 slab specimens. The 10 slab specimens were divided into two series (F09 and F14) depending on their flexural reinforcement ratios. There are five specimens in each series. The label of each specimen (for example, F*xx*-*yy*) indicates the values of its respective reinforcement ratio and fiber volume fraction, where *xx* represents the value of reinforcement ratio ρ (%) and *yy* represent the value of fiber volume fraction V_f (%).

Material properties

Steel fibers—The new double-hooked-end steel fibers[28] are shown in Fig. 1(a) and they have the following geometric properties: fiber length L_f is 60 mm (2.36 in.), fiber diameter D_f is 0.9 mm (0.035 in.), and the corresponding aspect ratio L_f/D_f is 65.[28] The nominal tensile strength of the steel fibers is 2300 MPa (333.6 ksi) and their modulus of elasticity is 210 GPa (30,460 ksi). For comparison, the typical single-hooked-end steel fiber[28] is shown in Fig. 1(b).

Steel reinforcements—Three different diameters of steel reinforcing bars were used: T10 (diameter = 10 mm [0.39 in.] or approximately No. 3 bars), T13 (diameter = 13 mm [0.51 in.] or approximately No. 4 bars), and T16 (diameter = 16 mm [0.63 in.] or approximately No. 5 bars). T10 is used for the bottom reinforcement for all 10 specimens, T13 is used for the top tension reinforcement for the F09 series specimens (ρ = 0.9%), and T16 is used for the top tension reinforcement for the F14 series specimens (ρ = 1.4%). The modulus of elasticity E_s, the yield strain ε_y, and the yield strength f_y are shown as follows:

For T10, E_s = 191 GPa (27,695 ksi), ε_y = 0.30%, f_y = 595 MPa (86.3 ksi)

For T13, E_s = 195 GPa (28,275 ksi), ε_y = 0.33%, f_y = 585 MPa (84.8 ksi)

For T16, E_s = 200 GPa (29,000 ksi), ε_y = 0.33%, f_y = 575 MPa (83.4 ksi)

Concrete—Columns 7 to 12 of Table 1 summarize the test results of the relevant concrete properties needed for the design of SFRC slabs. The compressive strengths f_c' were shown to increase slightly with an increase in fiber content (refer to Column 7). The flexural tensile tests were conducted according to the notched beam test of EN 14651.[25] Figure 2(a) shows the flexural stress-CMOD curves of the four batches of SFRC (each batch is according to its fiber volume fraction, V_f). The CMOD is the crack mouth opening displacement, as defined in EN 14651.[25] Figure 2(a) also shows that the double-hooked-end SFRC even at a fiber content as low as 0.3% shows enhanced performance over a non-fibrous beam whose curve would drop to zero stress immediately after reaching the peak stress. The double-hooked-end SFRC also shows better ductility than single-hooked end SFRC shown in Fig. 2(b). Note that the higher peak stress of the single-hooked end SFRC in Fig. 2(b) might have been caused by unintentional concentration of fibers above the notched zones of the test beams.

Table 1—Properties of SFRC slab specimens

Series	ID	c, mm (in.)	d, mm (in.)	ρ, %	f_y, MPa (ksi)	f_c', MPa (psi)	V_f, %	Residual tensile strength of SFRC				Reinforcing bar layout, mm (in.)
								f_{r1}, MPa (psi)	f_{r2}, MPa (psi)	f_{r3}, MPa (psi)	f_{r4}, MPa (psi)	
1	2	3	4	5	6	7	8	9	10	11	12	13
F09	F09-00	200 (7.9)	117 (4.6)	0.9	585 (84.8)	80 (11,600)	—	—	—	—	—	T13 @ 118 (No. 4 @ 4.6 in.)
	F09-03					89 (12,905)	0.3	4.2 (609)	6.0 (870)	6.5 (942.5)	5.8 (841)	
	F09-06					87 (12,615)	0.6	8.9 (1290)	12.8 (1856)	10.5 (1522.5)	7.5 (1087.5)	
	F09-09					90 (13,050)	0.9	16.0 (2320)	17.5 (2537.5)	16.3 (2363.5)	13.5 (1957.5)	
	F09-12					100 (14,500)	1.2	17.5 (2537)	21.2 (3074)	22.2 (3219)	21.2 (3074)	
F14	F14-00		114 (4.6)	1.4	575 (83.4)	80 (11,600)	—	—	—	—	—	T16 @ 118 (No. 5 @ 4.6 in.)
	F14-03					89 (12,905)	0.3	4.2 (609)	6.0 (870)	6.5 (942.5)	5.8 (841)	
	F14-06					87 (12,615)	0.6	8.9 (1290)	12.8 (1856)	10.5 (1522.5)	7.5 (1087.5)	
	F14-09					90 (13,050)	0.9	16.0 (2320)	17.5 (2537.5)	16.3 (2363.5)	13.5 (1957.5)	
	F14-12					100 (14,500)	1.2	17.5 (2537)	21.2 (3074)	22.2 (3219)	21.2 (3074)	

Notes: Concrete cover = 20 mm (0.8 in.); maximum aggregate size = 20 mm (0.8 in.); c is length of square column section; d is average effective depth; same reinforcement is provided in both directions; ρ is average reinforcement ratio $(\rho_x + \rho_y)/2$; $\rho_x = 100A_{sx}/(L_x \times d_x)$; L_x is length of slab specimen in x-direction; d_x is effective depth for x-direction; f_y is yield strength of flexural reinforcement; f_c' is cylinder compressive strength of concrete; f_{r1} to f_{r4} are residual flexural tensile strength corresponding with CMOD = 0.5, 1.5, 2.5, and 3.5 mm (0.02, 0.06, 0.10, and 0.14 in.), respectively, as defined by EN 14651[25]; T13 @ 118 or No. 4 @ 4.6 indicates deformed bars of 13 mm (1/2 in.) diameter distributed at 118 mm (4.6 in.) spacing on both directions.

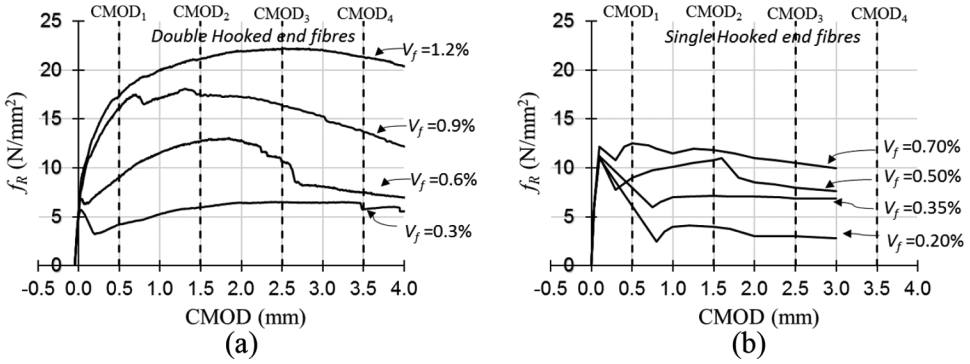

Fig. 2—Flexural tensile stress-CMOD curves of (a) SFRC using double-hooked-end fibers for V_f *= 0.3%, 0.6%, 0.9%, and 1.2%; and (b) SFRC using single hooked end fibers for* V_f *= 0.2%, 0.35%, 0.50%, and 0.70%. (Note: 1 mm = 0.0394 in.; 1 N/mm² = 145.04 psi.)*

Slab specimen details

Figure 3(a) shows the overall dimensions of the specimens. The overall size (L_1 x L_2 x h) of the specimens were 2.2 x 2.2 x 0.15 m (87 x 87 x 5.9 in.). The cross section of the column stub was 200 x 200 mm (7.9 x 7.9 in.). The height of the column stub was also 200 mm (7.9 in.) for all specimens. Figure 3(b) shows the reinforcement details of the 10 slab specimens. The diameter and spacing of the top flexural reinforcement for each specimen are given in Column 13 of Table 1. All specimens were provided with bottom reinforcement in the form of 10 bars of 10 mm diameter (0.39 in. or No. 3) in each direction.

Test setup and instrumentation

A typical test setup is shown in Fig. 4(a). Each specimen was placed on a steel support block. During testing, the specimen was vertically loaded downward through four hydraulic jacks that were secured onto the laboratory strong floor. Each hydraulic jack would apply the loading by pulling down the steel rod which transferred the pull-down force to the spreader beam and then on to the loading plates (points) on the slab. One load cell was placed on top of each spreader beam to measure and monitor the real-time pull-down force. The actual positions of the spreader beams and loading points (Fig. 3(a)) were determined by analyzing the

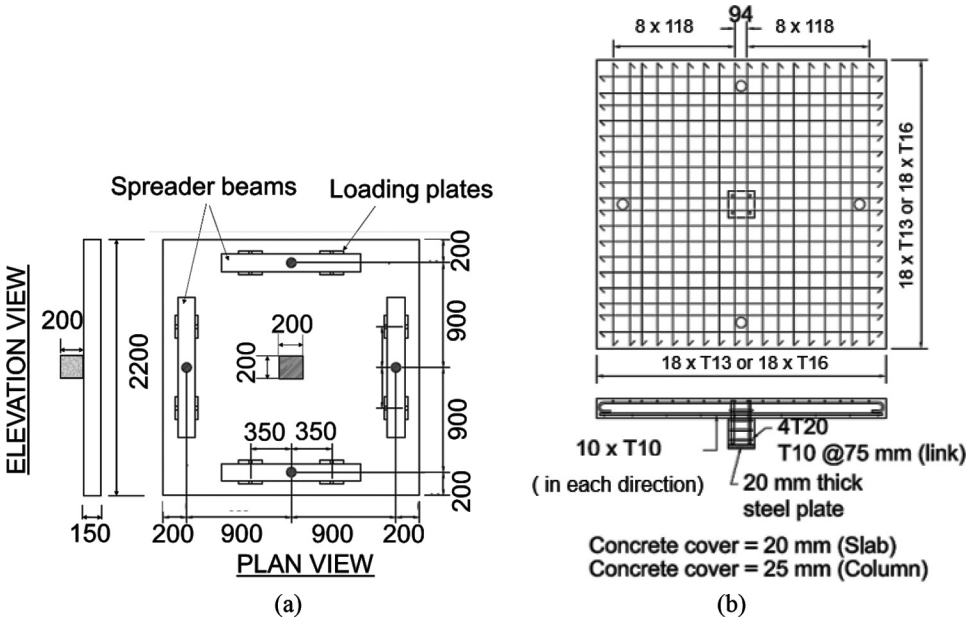

Fig. 3—(a) General dimension and loading positions; and (b) reinforcement details. (Note: Dimensions in mm; 1 mm = 0.0394 in.)

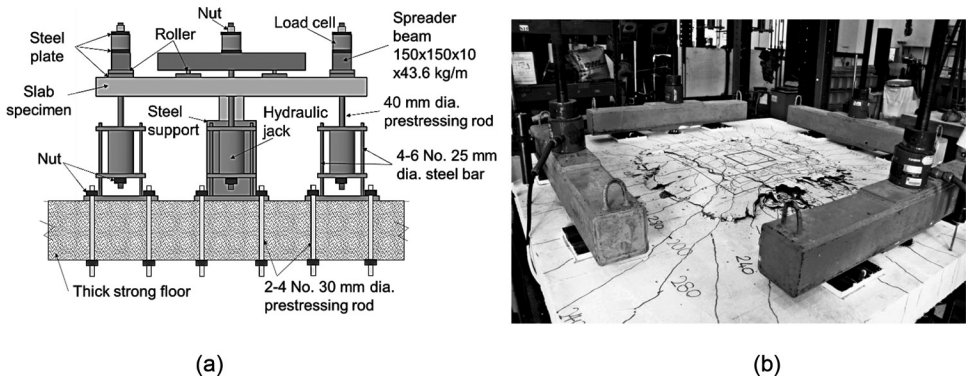

Fig. 4—(a) Typical test setup; and (b) photograph of Specimen F09-06 after test. (Note: 1 mm = 0.0394 in.; 1 kg/m = 0.67 lb/ft.)

slab using an elastic finite element program such that the distributions of stresses near the column zone were close to the stress distributions in the same slab under uniform loading. Figure 4(b) shows Specimen F09-06 after test.

Steel strain gauges were attached onto top reinforcing bars as shown in Fig. 5(a). To study the effectiveness of the steel reinforcement, the positions of strain gauges were determined such that they measure the strains in the reinforcements at appropriate spacings from column face. The labels of the strain gauges represent their coordinates (row, column); for example, G23 represents the strain gauge that is positioned at the second row and the third column as shown in Fig. 5(a). Twelve linear variable differential transformers (LVDTs) were installed to measure vertical deflections at various positions as shown in Fig. 5(b). Each LVDT was placed below the slab and attached on its individually secured stand, except for LVDTs D9, D11, D13, and D15 which were placed on top of the slab, due to congestion in the space below the slab.

Loading and monitoring procedure

Each specimen was loaded at a slow rate at the beginning to observe first flexural cracks. All the first cracks were observed carefully and crack propagations were marked using color markers. At every load increment, readings of vertical displacements from LVDTs, steel strains, and crack widths were recorded. All SFRC slabs were loaded beyond the maximum loads (failure loads) to capture post-failure behaviors.

EXPERIMENTAL RESULTS

Crack propagations and crack widths

Figure 6(a) shows the crack patterns of F09-series slabs at the ultimate load stage. The crack patterns of F14 series slabs are similar to the F09 series slabs and are shown in Fig. 6(b). The crack patterns and crack propagations of the SFRC slabs are somewhat similar to those of non-fibrous slabs failing in typical punching shear mode. The first cracks to form were the radial cracks originating from the column corners diagonally progress towards the edges of the slab, followed by flexural cracks around the column faces. As

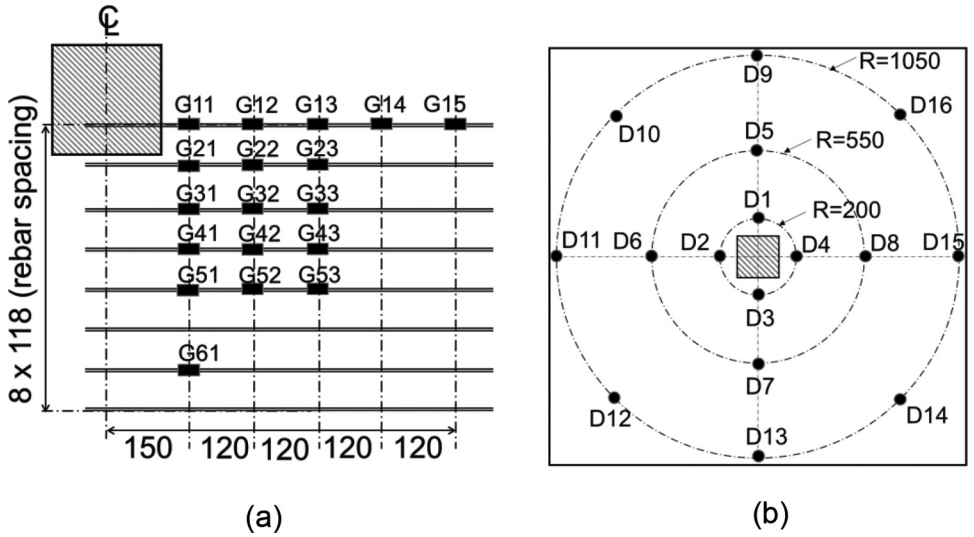

Fig. 5—(a) Typical arrangement of steel strain gauges; and (b) typical locations of LVDTs.

the load was increased, those radial cracks would progress to reach slab edges while other flexural (surface) cracks emanating from column faces would form. Circumferential cracks would subsequently develop upon further loading, making the appearance of small square patterns of cracks. Relatively more cracks at closer spacings would develop in SFRC slabs than in non-fibrous slabs. The widths of cracks are also narrower in SFRC slabs than in non-fibrous slabs. As the applied load approached the failure load, the final circumferential crack would appear, indicating that the internal inclined shear crack has reached top surface of the slab. Naturally, the internal inclined shear crack forms the final circumferential crack.

Crack widths were measured at various load stages for those cracks that were within the region of 200 mm (7.9 in.) away from column faces. It was observed that the widths of surface cracks were narrower for the slabs containing higher fiber volume fractions V_f than those with lower V_f at all load stages. At a specific load level, more cracks but with narrower crack width would develop in specimens with higher V_f compared to specimens with lower V_f. Figure 7 shows the crack width development charts for all the 10 specimens.

Ultimate punching failure loads

Table 2 shows the loads at first cracks or first cracking load (Column 4) and the punching failure loads (Column 5). It can be seen that the first cracking load increased with an increase in the fiber volume fraction, in particular for the F09-series slabs (flexural reinforcement ratio $\rho = 0.9\%$). The load at first crack was between 100 and 120 kN (22.5 and 27 kip). The addition of fibers beyond V_f of 0.6% does not seem to provide significant increase in the cracking load compared to the first cracking load of the slab with V_f of 0.6%.

Column 5 of Table 2 shows that the ultimate punching failure loads of the 10 slabs were considerably influenced by the fiber volume fraction V_f. By varying the fiber content from V_f of 0% to 1.2%, the punching failure loads increased by 190% or from 382 to 731 kN (85.9 to 164.3 kip) for the F09-series slabs. The increase in the F14-series slabs are higher, with punching failure loads increasing by 256% from 382 to 977 kN (85.9 to 219.6 kip). Between the F09 series ($\rho = 0.9\%$) and F14 series ($\rho = 1.4\%$) specimens, the failure load increment due to the addition of steel fibers is steeper for slabs with higher ρ (F14 series), as shown in Column 6 of Table 2. Thus, as expected, the results highlight that the flexural reinforcement ratios influenced the punching failure loads of the SFRC slabs.

Failure modes

Table 2 (Column 7) lists the observed failure modes of the slabs. The plain, non-fibrous slabs (F09-00 and F14-00) failed immediately after the peak loads were reached, so they had "brittle punching" failure mode. The four slabs with $V_f = 0.3\%$ and 0.6% also failed in punching but they were more ductile than the slabs without steel fiber, so the failure modes of these slabs were described as "ductile punching". The other four slabs with $V_f = 0.9\%$ and 1.2% had an interesting failure mode. The punching failure occurred after the occurrence of flat portion in the load-deflection curve (refer to following discussion on load-deflection curves), which indicates some yielding of the flexural reinforcements. So, the failure mode of these slabs is termed "flexural-punching".

Load-deflection curves

The load-deflection curves of all the specimens are shown in Fig. 8 and 9. Figure 8(a) shows the complete curves of the F09-series slabs, while Fig. 8(b) shows the elastic region of Fig. 8(a). Figures 9(a) and (b) correspond to F14-series slabs.

As expected, the slabs exhibit a linear-elastic behavior prior to cracking. Upon further loading, the slopes of the curves reduce and they become nonlinear as the flexural stiffness of the slabs continue to drop. The flexural stiffness of the slabs with higher flexural reinforcement ratio degrades less after cracking. This can be seen by comparing Fig. 9 and 8, in which the slopes of the F14 series slabs (Fig. 9) are steeper than the slopes of F09 series slabs (Fig. 8). The flexural stiffnesses of the slabs after cracking are also higher with increasing fiber volume fraction, as shown in Fig. 8(b)

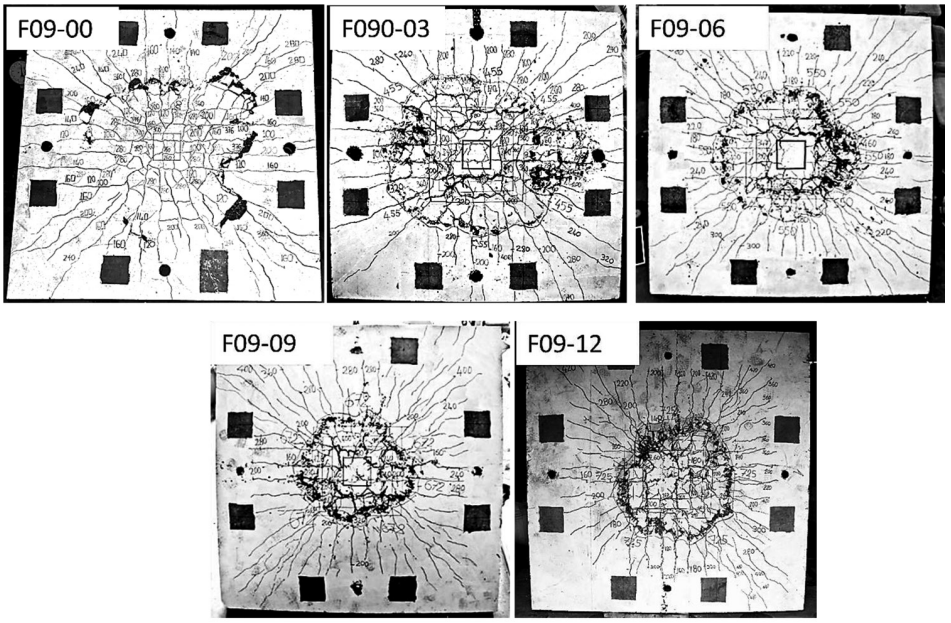

(a)

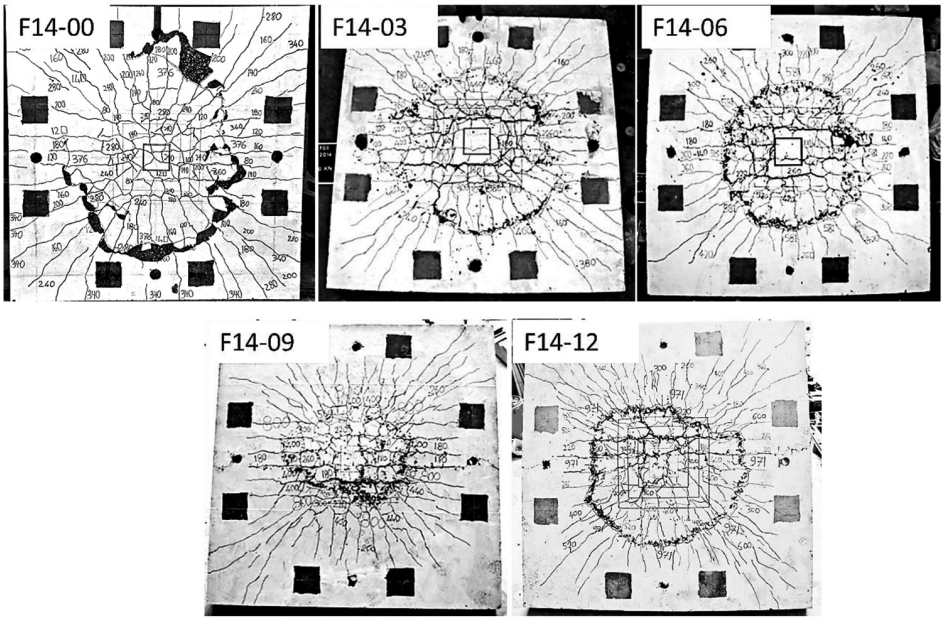

(b)

Fig. 6—(a) Ultimate cracks patterns of: (a) F09 series specimens; and (b) F14 series specimens. (Note: Top left labels are specimen IDs.)

and 9(b). This increases for a given value of ρ is due to the crack bridging of the fibers that was also observed in the notched beam tests shown in Fig. 2. This crack bridging makes the crack widths of SFRC slabs narrower than those of non-fibrous concrete slabs. Thus, the use of fibers can indeed improve slab performance at the service load level by reducing crack widths and maintaining stiffness after cracking.

At approximately 90% of failure load, the load-deflection curves for Specimens F09-09, F09-12, F14-09, and F14-12 become nearly flat. This indicates that yielding of the flexural reinforcement has occurred.

Figures 8(a) and 9(a) show that after failure the slabs containing steel fibers, even at fiber volume fraction V_f of only 0.3%, can still carry approximately 60% of their corresponding peak loads. They can carry this level of loads for considerable amount of slab deformations until the experiment was stopped. This shows that the double-hooked-end SFRC slabs can continue to carry their service loads even after experiencing punching failure.

Strains in flexural reinforcements

Figures 10 and 11 show the strains in the flexural reinforcements in F09 series and F14 series slabs, respectively. Figures 10(a) and 11(a) show the steel strains at failures of

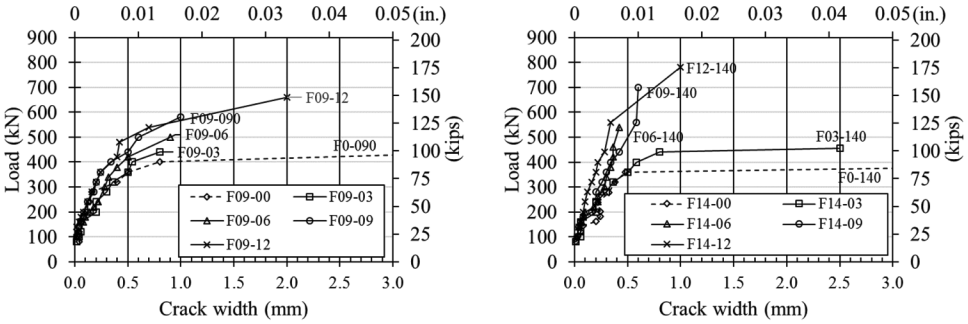

Fig. 7—Cracks widths in: (a) F09 specimens; and (b) F14 specimens.

Table 2—Experimental results of SFRC slabs

ID	ρ, %	V_f, %	Load at first crack, kN (kip)	Punching failure load V_{exp}, kN (kip)	Percentage increase in failure load, %	Observed failure mode
1	2	3	4	5	6	7
F09-00	0.9	—	60 (13.5)	381.7 (85.8)	—	Brittle punching
F09-03		0.3	80 (18.0)	461 (103.6)	21	Ductile punching
F09-06		0.6	100 (22.5)	556 (125.0)	46	Ductile punching
F09-09		0.9	100 (22.5)	678 (152.4)	77	Flexural punching
F09-12		1.2	120 (27.0)	731 (164.3)	91	Flexural punching
F14-00	1.4	—	80 (18.0)	382.3 (85.9)	—	Brittle punching
F14-03		0.3	80 (18.0)	466 (104.8)	22	Ductile punching
F14-06		0.6	100 (22.5)	587 (132.0)	55	Ductile punching
F14-09		0.9	100 (22.5)	806 (181.2)	111	Flexural punching
F14-12		1.2	100 (22.5)	977 (219.6)	156	Flexural punching

Notes: V_{exp} in Column 5 is failure load plus self-weight of slab outside perimeter measured at d away from column faces and weight of test equipment placed on top of slab.

the first set of the strain gauges (G11 to G61). Similarly, Fig. 10(b) and 11(b) show the steel strains of the second set of the strain gauges (G12 to G52). These sets of strain gauges were intended to capture flexural strains in the high shear and high moment regions; that is, at the distance of roughly 50 to 170 mm (1.9 to 6.7 in.) or roughly 0.5d to 1.5d from column face and/or where the flexural reinforcements are located.

Figures 10 and 11 show that flexural reinforcements in the non-fibrous slabs (F09-00 and F14-00) did not yield at failure, while the flexural reinforcements in the fiber reinforced concrete slabs yielded. The yielding of the flexural reinforcements became more widespread as the V_f increased from 0.3% to 1.2%, as shown in Fig. 10(a) and 11(a). Note, however, that the failure loads of slabs with higher V_f are much higher than those of non-fibrous slabs. As expected, the reinforcements in the F09-series slabs (ρ = 0.9%) reached the yield strains at a lower load than the F14-series slabs, and the strain values at any loading stage (after first cracks) were also higher in the F09-series slabs than in the F14-series slabs. At failure, the strains in the reinforcements of slabs with V_f = 0.9% and 1.2%, exceeded the yield strain even at locations near the edge of the slabs (Fig. 10(b) and 11(b)). Therefore, it is clear that the initial failure modes of the double-hooked-end SFRC slabs are flexure, which were also indicated by the flat portions in the load-deflection curves shown earlier in Fig. 8 and 9.

Comparison with other slabs using hooked-end fibers

From the experimental results, it is clear that the inclusion of double hooked-end fibers can increase the failure loads or shear resistance of concrete slabs significantly. The increase in the shear resistance of the slabs are proportional to the amount of the steel fiber added and the flexural reinforcement ratios ρ.

It is known that different types of fibers have different influences on the slab failure loads. Hence, to compare the effects of the two types of fibers on the punching shear strength, the chart in Fig. 12(a) was plotted to show the relationship between the normalized shear stress at failure $V_{exp}/(b_o d\sqrt{f_c'})$ in the y-axis to match the ACI formula and the fiber volume fraction V_f in the x-axis. Figure 12(b) is similar to Fig. 12(a), except that the y-axis is $V_{exp}/[ud\sqrt[3]{(100\rho f_c')}]$ instead, to match the Eurocode 2 formula. Note that b_o and u are the critical shear perimeters calculated according to ACI 318-14 (0.5d away from column face) and Eurocode 2 (2d away from column face with round corners), respectively. The data for comparison were obtained from Harajli et al.[19] and Gouveia et al.,[21] in addition to the authors' experiment. Relevant properties of the concrete and slab specimens are also provided in the legend of Fig. 12. Note that the authors used double-hooked-end fibers while Harajli et al.[19] and Gouveia et al.[21] used single-hooked-end fibers. The

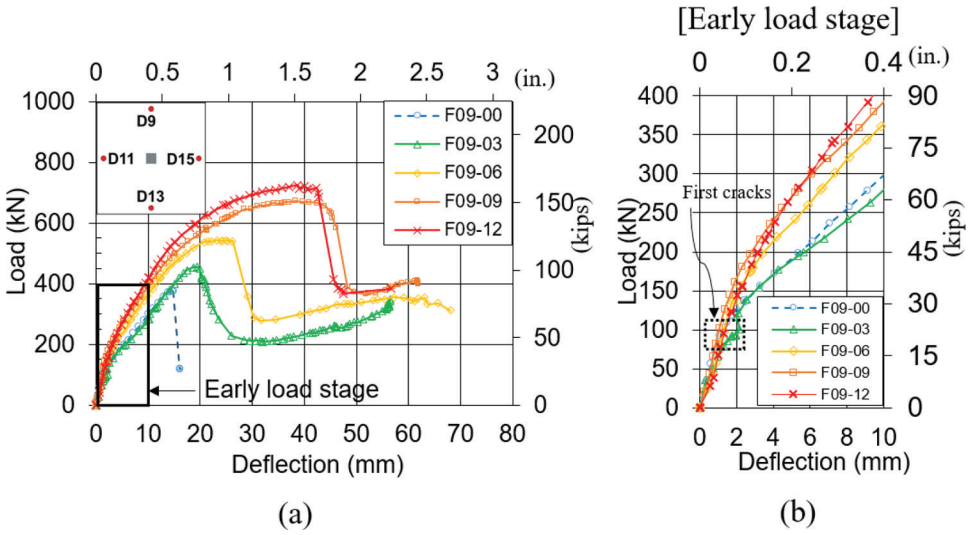

Fig. 8—Load-deflection curves of F09 series slabs: (a) full curves; and (b) early load stage. (Note: Deflection is average of four deflections at D9, D11, D13, and, D15 of Fig. 5(b).)

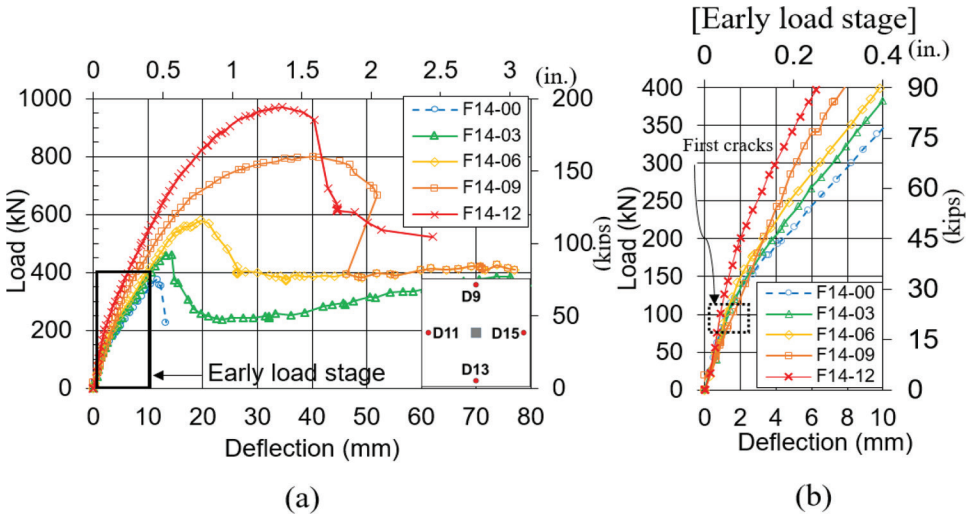

Fig. 9—Load-deflection curves of F14 series slabs: (a) full curves; and (b) early load stage. (Note: Deflection is average of four deflections at D9, D11, D13, and D15 of Fig. 5(b).)

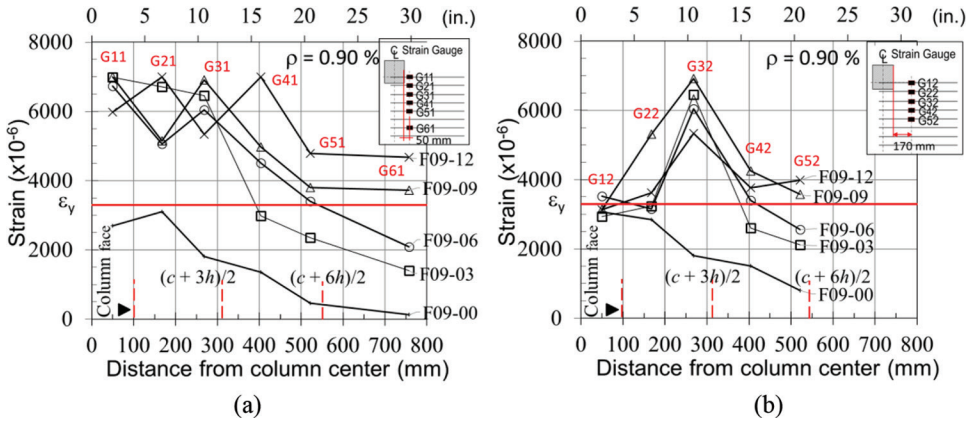

Fig. 10—Strain distributions of F09 series slabs at failure: (a) strain locations at 50 mm (1.97 in.) from line of column face; and (b) strain locations at 170 mm (6.69 in.) from line of column face.

relationships (trend lines) shown in Fig. 12 confirm that the punching shear strength of a slab, in general, increases with an increase in fiber volume fraction. The calculated shear strength according to ACI 318-14 and Eurocode 2 are also shown in Fig. 12(a) and (b), respectively, for rough comparison purposes. From Fig. 12(a) and (b), it can be seen that a

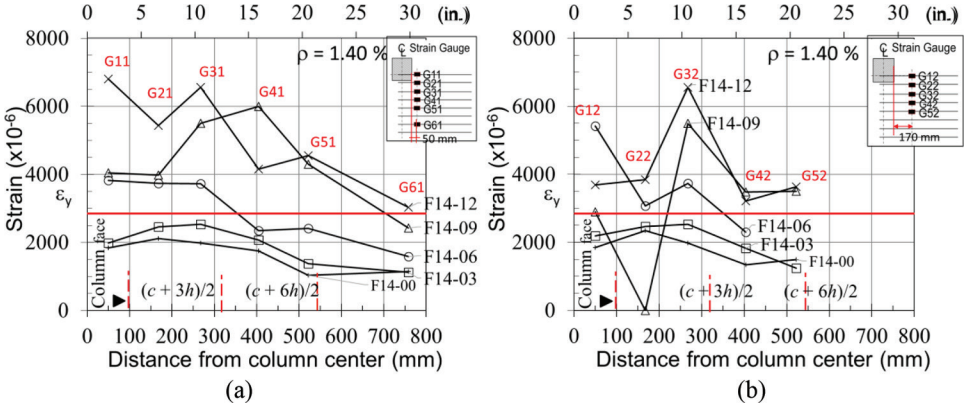

Fig. 11—Strain distributions of F14 series slabs at failure: (a) strain locations at 50 mm (1.97 in.) from line of column face; and (b) strain locations at 170 mm (6.69 in.) from line of column face.

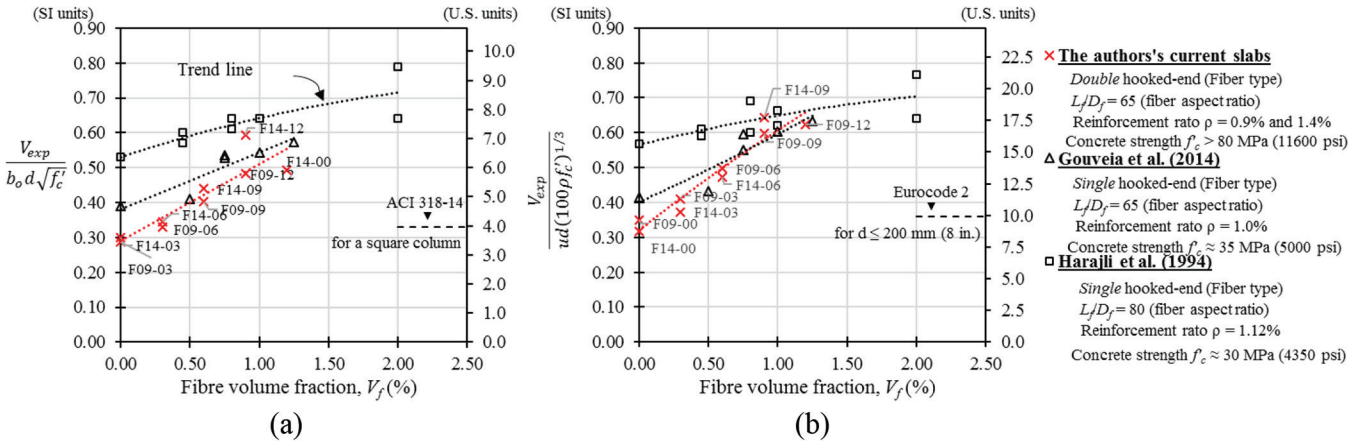

Fig. 12—Relationship between normalized punching shear stress at failure with fiber volume fraction V_f.

rise in the shear resistance of the authors' 10 slabs is particularly steeper than those of other slabs from Harajli et al.[19] and Gouveia et al.[21] An average increase in the punching shear strength of Harajli et al.'s slabs is approximately 35% (Fig. 12(a)), or 25% according to Fig. 12(b) when the fiber volume fraction increases from zero to 2% (with ρ = 1.12%, L_f/D_f = 80). The punching shear strength increases by 50% (Fig. 12(a)) or 65% (Fig. 12(b)) for Gouveia et al.'s slabs when the fiber volume fraction increases from zero to 1.0% (with ρ = 1%, L_f/D_f = 65). For the authors' slabs, the average increase is approximately 95% (Fig. 12(a)) or 110% (Fig. 12(b)) when the fiber volume fraction increases from 0.0 to 1.2%. As shown earlier in Table 2, however, that the punching shear strength of the authors' F14-12 slab (V_f = 1.2%) is approximately 156% higher than the strength of the non-fibrous slab (F14-00).

These comparisons show that the double hooked-end steel fibers have stronger positive effects on the punching shear strength of SFRC slabs than the single-hooked-end fibers. This is caused by the end shape of the fibers. The shape of a double-hooked-end steel fiber is such that its end forms a double hook, which can provide a stronger bond and thus less slippage compared to the end part of a normal single-hooked-end fiber (refer to Fig 1). This means that the double-hooked-end fibers also have better frictional or pullout resistance and better anchorage strength compared to the single-hooked-end fibers. Thus, the stress that can develop in the double-hooked-end fibers can be higher than the stress in the single-hooked-end fibers.

DESIGN METHODS AND YIELD LINE ANALYSIS

The methods described in the following are chosen because they are the more recent methods and they use more representative material properties to calculate the punching shear strength. Those material properties are the residual tensile strengths of the steel fiber reinforced concrete that are obtained by flexural tensile tests of a series of notched SFRC prisms. In this research, the flexural tensile tests were done according to EN 14651.[25] The residual tensile strengths will be able to show the influence of fiber volume fraction V_f more directly. The use of residual tensile strengths in calculating the ultimate punching shear strengths of SFRC slabs also eliminates the need to differentiate between different types of fibers as the performance of different fibers in tension is known directly.

Technical Report 34 by the Concrete Society[4]

The Concrete Society's TR 34[4] provides a design equation for calculating the punching shear strength of a fiber-reinforced concrete (FRC) slab. The method is based on the Eurocode 2[10] (EC2) equation and the design recommendations by RILEM.[24] The punching shear strength comprises of two components: the shear strengths contributed by the non-fibrous reinforced concrete, v_c (EC2's shear strength

equation), and the strength contributed by the FRC, v_f. TR 34 recommends to use only 50% of the RILEM's shear strength for FRC beams or $v_f = 0.5 \times 0.12 f_r$. The method can be summarized as follows

$$V_{Rd,TR34} = (v_c + v_f)ud \quad (1)$$

where

$$v_c = 0.18k(100\rho f_c')^{1/3} \text{ (in SI units)} \quad (2)$$

$$v_f = 0.5 \times 0.12 f_r = 0.06 f_r \text{ (in SI units)} \quad (3)$$

$$f_r = (1/4)(f_{r1} + f_{r2} + f_{r3} + f_{r4}) \quad (4)$$

The parameter u is the critical shear perimeter and it is calculated at a distance of $2d$ from column faces and it has round corners. k is the size effect coefficient: $k = 1 + \sqrt{200/d} \le 2.0$. The ρ is the average flexural reinforcement ratio ($\rho = \sqrt{\rho_x \rho_y} \le 0.02$). The average residual flexural strength f_r is taken to be the average value of f_{r1}, f_{r2}, f_{r3}, and f_{r4}, which are the residual flexural strengths corresponding to CMOD of 0.5, 1.5, 2.5, and 3.5 mm (0.02, 0.06, 0.10, and 0.14 in.), respectively. Some results of flexural tensile tests of the authors' SFRC prisms or beams are shown in Fig. 2.

Model Code 2010[11]

The Model Code 2010's simple equation for the punching shear strength of a FRC slab is shown in Eq. (5). Similar to the TR34, the shear strength contributed by the FRC v_f is simply added to the basic shear strength of non-fibrous reinforced concrete v_c to become the total punching shear strength V_{Rd} as given by

$$V_{Rd,MC2010} = (v_c + v_f)b_o d \quad (5)$$

The basic punching shear strength v_c here is based on the Critical Shear Crack Theory[30] and is given in Eq. (6). The punching shear strength is a function of $\sqrt{f_c'}$ and the factor $= 1/[1.5+0.9k_{dg}\psi d]$, which is a factor accounting for the opening and the roughness of the cracks.

$$v_c = \frac{1}{1.5 + 0.9k_{dg}\psi d}\sqrt{f_c'} \le 0.6\sqrt{f_c'} \text{ (in SI units)} \quad (6)$$

$$\psi = 1.5\frac{r_s}{d}\frac{f_y}{E_s} \quad (7)$$

$$k_{dg} = \frac{32}{16 + d_a} \quad (8)$$

where the slab rotation ψ (Eq. (7)) is the simplest form of equations for approximating the rotation of a slab provided in Model Code 2010. Other robust forms of equations need an iterative analysis. The basic control perimeter b_o has round corners and it is calculated at $d/2$ away from the column faces. k_{dg} is the size effect factor that depends on the maximum aggregate size d_a. r_s is the radius of the slab (= half of a slab length or $0.22L$) where L is column-to-column span. The maximum value of $\sqrt{f_c'}$ in Eq. (6) is limited to 8.0 MPa (1160.3 psi). In Eq. (8), d_a is taken to be zero for high-strength concrete ($f_c' > 70$ MPa [10152.6 psi]) and for lightweight concrete.

The shear strength contribution due to the presence of FRC v_f can be derived based on the simplified post-cracking constitutive laws in Sect 5.8 of the Model Code 2010.[11] Model Code 2010[11] provides two equations for calculating v_f. The first equation shown in Eq. (9) is based on the constitutive law called "rigid-plastic model" in which the residual tensile stress is assumed a constant ($= f_{r3}/3$) at any crack opening. The second equation shown in Eq. (10) is based on the "linear model" where the residual tensile stress is $0.45f_{r1}$ at the tip of crack opening and linearly proportional to the maximum crack opening w_u, with the w_u taken to be 1.5 mm (0.06 in.). The two equations of v_f are

$$v_f = \frac{f_r}{3} \text{ (Rigid plastic model)} \quad (9)$$

$$v_f = 0.45f_{r1} - \frac{w_u}{2.5}(0.65f_{r1} - 0.5f_{r3}) \text{ (Linear model)} \quad (10)$$

The second equation of v_f in Eq. (10) considers the post-crack hardening and post-crack softening behaviors of the cracked FRC members. Since these post-crack behaviors were observed and discussed earlier (refer to Fig. 2(a)), the authors use v_f in Eq. (10) for the Model Code 2010's method in the subsequent analysis and comparison with the test results.

Yield line theory[29]

ACI 544.6R[1] has provided several design approaches for evaluating the flexural strength of SFRC slabs, in which the yield line theory[29] is used as the basis. In this paper, the flexural strength V_{flex} of a slab is defined as the applied shear force that causes flexural failure of the slab, and V_{flex} can be calculated using the yield line theory. One of the challenges in yield line analysis is to identify the correct and admissible yield line pattern of a slab that can represent the actual failure mechanism. An admissible yield line pattern is very much influenced by various factors such as slab geometry, reinforcement ratio, and loading condition. However, for a slab loaded on the column, the V_{flex} can typically be determined from the so-called "circular fan" yield line pattern, which is also suggested in ACI 544.6R.[1] This yield line pattern is similar (though different in diameter) to the actual crack patterns of the authors' slabs that have ductile failures (Slabs F09-09, F09-12, F14-09, and F14-12).

The equation of V_{flex} for the circular fan pattern is[31]

$$V_{flex} = m_u\left[\frac{2(c_1 + c_2)}{r} + 2\pi\right] \quad (11)$$

where c_1 and c_2 are the lengths of long and short sides of column section, respectively. For the current analysis, c_1 and c_2 become c, which is the side length of a square column. r is the distance from the column face to the point load (for

design purposes, r can also be assumed to be $0.2L$, with L being the column-to-column span). The derivation of the corresponding V_{flex} can be obtained in the book by Park and Gamble.[31] The ultimate moment capacity m_u per unit width is given in Eq. (12) and (13). For a non-fibrous RC member, the moment capacity m_u can be calculated as follows

$$m_u = \rho d^2 f_y \left(1 - 0.59 \frac{\rho f_y}{f'_c}\right)$$

(For non-fibrous RC members) (12)

There is no standard design rule for calculating the moment capacity of SFRC members yet. According to TR 34,[4] the classical beam bending approach can be used to derive a standard equation for calculating the ultimate moment capacity per unit width for a SFRC member, where tension-controlled failure is assumed. The concrete tensile stress along crack openings is included in the analysis and that leads to the following equation[4]

$$m_u = h^2 \left(0.16\sigma_{r1} + 0.29\sigma_{r4}\right) + \rho d^2 f_y \left(1 - 0.048 \frac{h}{d}\right)$$
$$= h^2 \left(0.072 f_{r1} + 0.107 f_{r4}\right) + \rho d^2 f_y \left(1 - 0.048 \frac{h}{d}\right)$$

(For FRC members) (13)

where σ_{r1} (= $0.45f_{r1}$) and σ_{r4} (= $0.37f_{r4}$) are the equivalent tensile stresses[24] at the neutral axis (tip of the crack opening) and at the maximum crack opening at the tension face, respectively. f_{r1} and f_{r4} are obtained from the notched beam tests done according to EN 14651[25] and they are the residual tensile strengths corresponding to the CMOD of 0.5 and 3.5 mm (0.0197 and 0.138 in.), respectively. A more complex form of m_u is also provided in TR34,[4] which requires iterative procedure. For verification and comparison purposes in this study, the authors used the simple equations of m_u given in Eq. (12) and (13) in the subsequent analysis.

COMPARISONS OF DESIGN METHODS WITH TEST RESULTS

Table 3 shows the comparisons and verifications of the performance of Model Code 2010[11] method, TR 34[4] method, as well as the yield line theory (V_{flex}) with the current 10 slabs. For the purpose of comparisons in this section, all the load factors, materials safety factors, and strength reduction factors are set equal to 1.0. The failure load of each specimen V_{exp} includes the self-weight of the slab outside the perimeter measured at d away from the column faces and the weight of test equipment placed on top of the slab. The performance of each method will be evaluated by statistical analysis of the ratio of the experimental failure load to the calculated failure load (V_{exp}/V_{calc}).

Performance of yield line theory

The analysis results in Columns 2 and 4 of Table 3 show the failure loads V_{exp} of the slabs and the calculated strength V_{flex} using the yield line theory. The ratios of $V_{exp}/V_{calc,}$ shown in Column 11, are significantly lower than 1.0 (average V_{exp}/V_{calc} = 0.71). This indicates that the punching shear strength calculated by the yield line theory (V_{flex}) overestimates the actual strength significantly. It was discussed earlier that the failures of the slabs with a high fiber volume fraction such as F09-09, F09-12, F14-09, and F14-12 were initiated by flexure. Obviously, the failure might have involved more than just simple "circular fan" type flexure failure, but also other factors as well. The authors have earlier discussed some of the factors affecting flexural failures for non-fibrous slabs in Ref. 32. The presence of high bending moment in the same location as high shear force is an important factor. It may cause the slabs to fail at lower loads then slabs subjected to high bending moment but low shear force. The double-hooked-end fibers are also a recent invention.[28] All these factors, including the fact that punching stresses are three dimensional, may affect the accuracy of the yield-line-theory based method.

Performance of TR34

The TR34 method performs the best among the three methods, with a coefficient of variation (COV) of only 12% and an average value of V_{exp}/V_{calc} of 0.99 (refer to Table 3, Column 12). The predicted increment in shear strength V_{Rf} (Column 6) due to an addition of the double hooked-end fibers is relatively consistent with the failure load increments ΔV of the slabs (shown in Column 3). Yet, in Column 12 of Table 3, the TR34's method is shown to overestimate slightly the strength of the slabs with low fiber volume fraction and slabs without fibers (F09-03, F09-00, F14-03 and F14-00). This is somewhat expected, because the TR34 method for non-fibrous slabs is essentially the Eurocode 2 method without the v_f term. The authors[32] have previously evaluated the performance of Eurocode 2 (EC2) for high strength non-fibrous concrete slabs. It was found that the EC2 equation tends to overestimate the strengths of the high-strength, non-fibrous concrete slabs, especially for concrete strength f_c' greater than 80 MPa (11,600 psi). Overall, nevertheless, the TR-34 method can be considered accurate.

Performance of Model Code 2010

The MC2010 method is less accurate compared to the other two methods. Even though its average V_{exp}/V_{calc} is 0.99, its COV is very large (44%; refer to Table 3, Column 13). The highly scattered predictions are because of the underestimation of the strengths of slabs without fibers (maximum V_{exp}/V_{calc} of 1.81) and overestimation of the strengths of slabs with fibers (minimum V_{exp}/V_{calc} of 0.58). The overly conservative prediction of the F09-00 and F14-00 can be due to the inaccuracy of the simplified formula for slab rotation ψ in Eq. (7). Yet, it is difficult to see the cause of inaccuracy without doing comprehensive study of the MC2010. Such study is not the intention of this paper. The more complex form of ψ in MC2010, which requires iterative procedures and considers the influence of reinforcement ratios, may increase accuracy. The MC2010 method considers the contribution of the fibers to punching shear strength through the V_{Rf} (= $v_f \times b_o d$) term. It can be seen in Column 9 of Table 3 that V_{Rf} terms are too high when compared to the

Table 3—Comparisons of design methods with experimental results

ID	V_{exp}, kN (kip)	ΔV, kN (kip)	V_{flex} Eq. (11), kN (kip)	TR34 V_c Eq. (2), kN (kip)	TR34 V_{Rf} Eq. (3), kN (kip)	TR34 V_{Rd} Eq. (1) [(5) + (6)], kN (kip)	MC2010 V_c Eq. (6), kN (kip)	MC2010 V_{Rf} Eq. (10), kN (kip)	MC2010 V_{Rd} Eq. (5) [(8) + (9)], kN (kip)	V_{exp}/V_{calc} YLT [(2)/(4)]	V_{exp}/V_{calc} TR34 [(2)/(7)]	V_{exp}/V_{calc} MC 2010 [(2)/(10)]
1	2	3	4	5	6	7	8	9	10	11	12	13
F09-00	381.7 (85.8)	—	505.4 (113.6)	398.0 (89.5)	—	398.0 (89.5)	212.4 (47.8)	—	212.4 (47.8)	0.76	0.96	1.80
F09-03	461 (103.6)	79 (17.8)	623.0 (140.1)	412.4 (92.7)	89.6 (20.1)	502.0 (113)	212.4 (47.8)	300.8 (67.6)	513.2 (115.4)	0.74	0.92	0.90
F09-06	556 (125.0)	174 (39.1)	701.8 (157.8)	409.3 (92.0)	158.1 (35.5)	567.4 (127.6)	212.4 (47.8)	503.3 (113.2)	715.7 (160.9)	0.79	0.98	0.78
F09-09	678 (152.4)	296 (66.5)	868.2 (195.2)	413.9 (93.1)	252.1 (56.7)	666.0 (149.7)	212.4 (47.8)	799.1 (179.7)	1011.6 (227.4)	0.78	1.02	0.67
F09-12	731 (164.3)	349 (78.5)	992.0 (223.0)	428.7 (96.4)	327.0 (73.5)	755.7 (169.9)	212.4 (47.8)	1053.2 (236.8)	1265.6 (284.5)	0.74	0.97	0.58
F14-00	382.3 (85.9)	—	716.4 (161.1)	440.6 (99.1)	—	440.6 (99.1)	211.5 (47.5)	—	211.5 (47.5)	0.53	0.87	1.81
F14-03	466 (104.8)	84 (18.9)	842.9 (189.5)	456.6 (102.7)	85.9 (19.3)	542.4 (121.9)	211.5 (47.5)	290.7 (65.4)	502.3 (112.9)	0.55	0.86	0.93
F14-06	587 (132.0)	205 (46.1)	921.8 (207.2)	453.1 (101.9)	151.5 (34.1)	604.6 (135.9)	211.5 (47.5)	486.4 (109.4)	697.9 (156.9)	0.64	0.97	0.84
F14-09	806 (181.2)	424 (95.3)	1088.2 (244.6)	458.3 (103.0)	241.6 (54.3)	699.9 (157.4)	211.5 (47.5)	772.4 (173.7)	983.9 (221.2)	0.74	1.15	0.82
F14-12	977 (219.6)	595 (134)	1211.9 (272.5)	474.7 (106.7)	313.3 (70.4)	788.0 (177.2)	211.5 (47.5)	1017.9 (228.8)	1229.5 (276.4)	0.81	1.24	0.79
									Minimum	0.53	0.86	0.58
									Maximum	0.81	1.24	1.81
									Average	0.71	0.99	0.99
									COV	0.139	0.120	0.44

Notes: V_{exp} in Column 2 is failure load plus self-weight of slab outside perimeter measured at d away from column faces and weight of test equipment placed on top of slab. ΔV in Column 3 is the failure load increment due to addition of fibers to base or non-fibrous slab in the series (either F09-00 or F14-00). $V_c = v_c \times (ud)$ or $v_c \times (b_o d)$ and $V_{Rf} = v_f \times (ud)$ or $v_f \times (b_o d)$.

actual increment of failure load due to the contribution of fiber, ΔV, shown in Column 3. This clearly indicates that MC2010 overestimates the contribution of the fibers.

CONCLUSIONS

Based on the experimental results reported herein and the accompanying discussions, the following conclusions can be drawn:

1. The punching shear strength of a slab can be significantly enhanced by the inclusion of steel fibers. The experimental results show that the punching shear strength of the double-hooked-end SFRC slabs having volume fraction of 1.2% can be on average more than 110% higher and up to even 156% higher individually than the strengths of similar non-fibrous concrete slabs of the same flexural reinforcement ratio. This is considerably higher than the increment introduced by conventional single-hooked-end steel fibers, which can increase punching shear strength on average by approximately 35 to 65%, depending on volume fraction and fiber aspect ratio.

2. After punching failure, the residual strength of double-hooked-end SFRC slabs is approximately 60% of their corresponding peak loads, even for those with low fiber volume fraction V_f of only 0.3%. This means that the double-hooked-end SFRC slabs can continue to carry their full service loads (approximately 60% of ultimate load) even after experiencing punching failure.

3. The addition of fibers can enhance the serviceability performance of the slabs. It can delay the occurence of first flexural cracks because the concrete flexural tensile strength or modulus of rupture is increased. The crack widths at all stages of loadings are reduced with an increase in the fiber volume fraction.

4. As the fiber volume fraction V_f increases, the ductility of the slab increases as well and its punching shear strength also increases. For a fiber volume fraction of 0.9% (fiber dosage = 70.2 kg/m^3 [4.5 lb/ft^3]) or higher, the punching failure mode of the slab, with flexural reinforcement ratio ρ of 1.4% or less, becomes very ductile as the failure is initiated by flexural failure before punching failure occurs.

5. The Concrete Society's TR 34 method is accurate for the current SFRC slabs. The method of the Model Code 2010, using the non-iterative approach, is inaccurate and unconservative for the current slabs. The method based on the yield

line theory, which is usually used for slabs failing in ductile punching as presented herein, is also unconservative as it overestimates the punching strength of all the SFRC slabs.

AUTHOR BIOS

Khatthanam Chanthabouala *is a Civil and Structural Engineer in Laos. He received his bachelor of engineering and doctor of philosophy degrees from Nanyang Technological University, Singapore. His research interests include the behavior of high-strength concrete slabs and steel fiber-reinforced concrete flat-plate structures.*

ACI member **Susanto Teng** *is an Associate Professor at Nanyang Technological University. He is a member of ACI Committee 435, Deflection, and Joint ACI-ASCE Committees 421, Design of Reinforced Concrete Slabs, and 445, Shear and Torsion. His research interests include design and behavior of concrete and fiber-reinforced concrete members including beams, slabs, and walls under static and dynamic loads; size effect in shear behavior; and finite element modeling of concrete structures.*

Jimmy Chandra *is a Lecturer at Petra Christian University, Surabaya, Indonesia. He received his bachelor of engineering degree from Petra Christian University; his master's degree from Asian Institute of Technology, Bangkok, Thailand; and his PhD from Nanyang Technological University. His research interests include the behavior and seismic performance evaluation of reinforced concrete structures.*

Kang-Hai Tan *is a Professor in the School of Civil and Environmental Engineering, Nanyang Technological University. His research interests include design and behavior of concrete deep beams, behavior of concrete and steel structures subjected to fire loading, fire engineering, modeling of structures under fire loading, and modeling of progressive collapse.*

Claudia P. Ostertag *holds the T.Y. and Margaret Lin Chair of Engineering in the Civil Engineering Department at the University of California, Berkeley, Berkeley, CA. She received her MS from the University of Stuttgart, Stuttgart, Germany, and her PhD from the University of California, Berkeley. Her research interests include toughening and strengthening mechanisms of fiber-reinforced composites and the effect of crack control on durability of cement-based materials.*

ACKNOWLEDGMENTS

The authors are grateful for the funding provided by the National Research Foundation (NRF) of Singapore through the Competitive Research Programme (CRP) "Underwater Infrastructure and Underwater City of the Future" and Nanyang Technological University, Singapore.

REFERENCES

1. ACI Committee 544, "Report on Design and Construction of Steel Fiber-Reinforced Concrete Elevated Slabs (ACI 544.6R-15)," American Concrete Institute, Farmington Hills, MI, 2015, 38 pp.

2. ACI Committee 544, "Design Considerations for Steel Fiber Reinforced Concrete (ACI 544.4R-88) (Reapproved 2009)," American Concrete Institute, Farmington Hills, MI, 1988, 18 pp.

3. ACI Comittee 544, "Guide for Specifying, Proportioning, and Production of Fiber-Reinforced Concrete (ACI 544.3R-08)," American Concrete Institute, Farmington Hills, MI, 2008, 16 pp.

4. TR 34, *Concrete Industrial Ground Floors: A Guide to Design and Construction*, fourth edition, The Concrete Society, Surrey, UK, 2016, 99 pp.

5. Chandler, J., and Neal, F., "The Design of Ground-Supported Concrete Industrial Floor Slabs," *Interim Technical Note 11*, Cement and Concrete Association, 1988, 16 pp.

6. Li, V. C., "Large Volume, High-Performance Applications of Fibers in Civil Engineering," *Journal of Applied Polymer Science*, V. 83, No. 3, 2002, pp. 660-686. doi: 10.1002/app.2263

7. Mobasher, B., and Destree, X., "Design and Construction Aspects of Steel Fiber-Reinforced Concrete Elevated Slabs," *Fiber-Reinforced Self-Consolidating Concrete: Research and Applications*, SP-274, American Concrete Institute, Farmington Hills, MI, 2010, pp. 95-108.

8. Henager, C. H., "Steel Fibrous Ductile Concrete Joint for Seismic Resistant Structures," *Reinforced Concrete Structures in Seismic Zones*, SP-53, American Concrete Institute, Farmington Hills, MI, 1977, pp. 371-386.

9. ACI Committee 318, "Building Code Requirements for Structural Concrete (ACI 318-14) and Commentary (ACI 318R-14)," American Concrete Institute, Farmington Hills, MI, 2014, 520 pp.

10. EN 1992-1-1, "Eurocode 2: Design of Concrete Structures: Part 1-1—General Rules and Rules for Buildings," European Committee for Standarization, Brussels, Belgium, 2004, 225 pp.

11. *fib* bulletin 65-66, "Model Code 2010, Final Draft," CEB-FIP, Lausanne, Switzerland, 2012.

12. Romualdi, J. P., and Mandel, J. A., "Tensile Strength of Concrete Affected by Uniformly Distributed and Closely Spaced Short Lengths of Wire Reinforcement," *ACI Journal Proceedings*, V. 61, No. 6, June 1964, pp. 657-672.

13. Swamy, R. N., and Mangat, P. S., "A Theory for the Flexural Strength of Steel Fiber Reinforced Concrete," *Cement and Concrete Research*, V. 4, No. 2, 1974, pp. 313-325. doi: 10.1016/0008-8846(74)90142-2

14. Swamy, R. N., and Ali, S. A. R., "Punching Shear Behavior of Reinforced Slab-Column Connections Made with Steel Fiber Concrete," *ACI Journal Proceedings*, V. 79, No. 5, Sept.-Oct. 1982, pp. 392-406.

15. Narayanan, R., and Darwish, I. Y. S., "Punching Shear Tests on Steel-Fiber Reinforced Micro-Concrete Slabs," *Magazine of Concrete Research*, V. 39, No. 138, 1987, pp. 42-50. doi: 10.1680/macr.1987.39.138.42

16. Theodorakopoulos, D., and Swamy, N., "Contribution of Steel Fibers to the Strength Characteristics of Lightweight Concrete Slab-Column Connections Failing in Punching Shear," *ACI Structural Journal*, V. 90, No. 4, July-Aug. 1993, pp. 342-355.

17. Alexander, S. D. B., and Simmonds, S. H., "Punching Shear Tests of Concrete Slab-Column Joints Containing Fiber Reinforcement," *ACI Structural Journal*, V. 89, No. 4, July-Aug. 1992, pp. 425-432.

18. Shaaban, A. M., and Gesund, H., "Punching Shear Strength of Steel Fiber Reinforced Concrete Flat Plates," *ACI Structural Journal*, V. 91, No. 4, July-Aug. 1994, pp. 406-414.

19. Harajli, M. H.; Maalouf, D.; and Khatib, H., "Effect of Fibers on the Punching Shear Strength of Slab-Column Connections," *Cement and Concrete Composites*, V. 17, No. 2, 1995, pp. 161-170. doi: 10.1016/0958-9465(94)00031-S

20. Higashiyama, H.; Ota, A.; and Mizukoshi, M., "Design Equation for Punching Shear Capacity of SFRC Slabs," *International Journal of Concrete Structures and Materials*, V. 5, No. 1, 2011, pp. 35-42. doi: 10.4334/IJCSM.2011.5.1.035

21. Gouveia, N. D.; Fernandes, N. A. G.; Faria, D. M. V.; Ramos, A. M. P.; and Lúcio, V. J. G., "SFRC Flat Slabs Punching Behaviour – Experimental Research," *Composites. Part B, Engineering*, V. 63, 2014, pp. 161-171. doi: 10.1016/j.compositesb.2014.04.005

22. Grimaldi, A.; Meda, A.; and Rinaldi, Z., "Experimental Behaviour of Fibre Reinforced Concrete Bridge Decks Subjected to Punching Shear," *Composites. Part B, Engineering*, V. 45, No. 1, 2013, pp. 811-820. doi: 10.1016/j.compositesb.2012.09.044

23. Caratelli, A.; Imperatore, S.; Meda, A.; and Rinaldi, Z., "Punching Shear Behavior of Lightweight Fiber Reinforced Concrete Slabs," *Composites. Part B, Engineering*, V. 99, 2016, pp. 257-265. doi: 10.1016/j.compositesb.2016.06.045

24. RILEM, "Final Recommendation of TC 162-TDF: Test and Design Methods for Steel Fibre Reinforced Concrete," *Materials and Structures*, V. 36, No. 262, 2003, pp. 560-565. doi: 10.1617/14007

25. BS EN 14651, "Test Method for Metallic Fibre Concrete—Measuring the Flexural Tensile Strength (Limit of Proportionality (LOP), Residual), British Standards Institution, London, UK, 2007.

26. Theodorakopoulos, D. D., and Swamy, R. N., "A Design Method for Punching Shear Strength of Steel Fiber Reinforced Concrete Slabs," *Innovations in Fiber-Reinforced Concrete for Value*, SP-216, American Concrete Institute, Farmington Hills, MI, 2003, pp. 181-202.

27. Maya, L. F.; Fernández Ruiz, M.; Muttoni, A.; and Foster, S. J., "Punching Shear Strength of Steel Fibre Reinforced Concrete Slabs," *Engineering Structures*, V. 40, 2012, pp. 83-94. doi: 10.1016/j.engstruct.2012.02.009

28. BEKAERT, Dramix 5D fibres Datasheet, https://www.bekaert.com/en/product-catalog/content/datasheets/Dramix5D.

29. Johansen, K. W., *Yield-Line Theory*, Cement and Concrete Association, London, UK, 1962, 181 pp.

30. Muttoni, A., "Punching Shear Strength of Reinforced Concrete Slabs without Transverse Reinforcement," *ACI Structural Journal*, V. 105, No. 4, July-Aug. 2008, pp. 440-450.

31. Park, R., and Gamble, W. L., *Reinforced Concrete Slabs*, John Wiley & Sons, New York, 2000.

32. Teng, S.; Chanthabouala, K.; Lim, T. Y.; and Hidayat, R., "Punching Shear Strength of Slabs and Influence of Low Reinforcement Ratio," *ACI Structural Journal*, V. 115, No. 1, 2018, pp. 139-150. doi: 10.14359/51701089